A Novel Glia-immune humanized mouse model for investigation of HIV CNS infection and neuroinflammation.

Shallu Tomer*[1], Lin Pan*[2], Jeffrey Harding[1], Valerie Rezek[1], Mitchell Krawczyk[2], Ethan Cook[1], Nandita Kedia[1], Li Wang[1], Jonathan Le[1], Heather Martin[1], Erik Gramajo[1], Xiang Li[2], Yewen Zhang[2], Wenli Mu[1], Jing Wen[3], Scott Kitchen[1], Ye Zhang[§2] & Anjie Zhen[§1]

[1] Division of Hematology and Oncology, David Geffen School of Medicine, University of California, Los Angeles

[2] Department of Psychiatry and Biobehavioral Sciences, David Geffen School of Medicine, University of California, Los Angeles

[3] Depart of Department of Microbiology, Immunology, & Molecular Genetics, University of California, Los Angeles

*Co-first authors

[§]Corresponding Authors: Anjie Zhen, azhen@mednet.ucla.edu, Ye Zhang, yezhang@ucla.edu

Abstract

Although combined antiretroviral therapy (ART) is successful in suppressing viral replication, HIV persists in anatomic reservoirs, including the central nervous system (CNS). Current models, such as HSC-reconstituted humanized mice, lack matched human glia in the brain, limiting insights into HIV CNS infection and pathogenesis. We developed a novel glia-immune humanized mouse model integrating human glial cells in the brain with donor-matched human immune reconstitution in peripheral blood and lymphoid tissues. Neonatal NSG mice were injected intrahepatically with Hematopoietic Stem Cells (HSCs) and intracranially with donor-matched glia. We observed extensive engraftment of

all three types of human glial cells (astrocytes, oligodendroglia, and microglia-like cells) in key CNS regions, including the cerebral cortex and hippocampus. These glia-immune mice supported robust HIV-1 replication in the peripheral blood, lymphoid tissues and CNS. HIV-infected mice exhibited heightened inflammation and elevated expression of type I interferon-stimulated genes (ISGs) in peripheral and brain tissues. Bulk RNAseq revealed significant transcriptional changes in human glia, such as upregulation of ISGs, inflammasome-associated genes, and downregulation of transcriptional regulators implicated in metabolic regulations and epigenetic controls. Overall, this model allows interrogation of glial transcriptomic changes and neuron-immune interactions, offering insights into HIV CNS infection, pathology, and therapeutic strategies targeting CNS HIV reservoirs and neuroinflammatory pathways.

34 **Introduction**

35 Despite development of effective combined anti-retroviral therapy (ART), HIV remains largely incurable
36 due to persistent viral reservoirs, including in the central nervous system (CNS). As many as 50% of
37 people living with HIV (PLWH) experience CNS comorbidities (ref). Compared to peripheral reservoirs,
38 our understandings of the infection and reservoirs in the CNS are limited. Pathogenesis of HIV infection
39 in the CNS is not fully understood but is multifactorial: HIV replicates and persists in the CNS resident
40 cells, viral proteins are neurotoxic, CNS inflammation occurs and many other pathogenic effects are
41 observed. While microglia appear to be the main HIV-1 reservoir in the brain[1], astrocytes and
42 oligodendroglia (including oligodendrocytes and oligodendrocyte precursor cells), may also be affected[2-
43 4]. Astrocytes are essential for brain homeostasis and can drive the induction and progression of a pro-
44 inflammatory environment (Ref). Damage to oligodendroglia and myelin has been detected in patients
45 with HIV, correlating with neurocognitive deficits (Ref). Therefore, understanding how infiltrating immune
46 cells and resident CNS glia - microglia, astrocytes, and oligodendroglia - support and respond to HIV
47 infection is critical for elucidating the pathogenesis of CNS comorbidity.
48
49 Commonly used platforms for studying HIV CNS infection and pathogenesis have limitations. HIV does
50 not productively infect mice or non-human primates (NHPs)[5], and obtaining HIV-infected human brain
51 tissues from people living with HIV (PWLH) is challenging. As a result, the molecular mechanisms of HIV
52 CNS infection and CNS pathogenesis remain largely elusive. Humanized mice transplanted with human
53 hematopoietic stem cells (HSCs) allow the development of a functional human immune system, support
54 robust HIV replication, and enable HIV latency establishment[6-11]. These models have proven valuable for
55 investigating HIV immunopathogenesis, latency reactivation and testing gene and cell therapies as
56 described in ours[6-8,12-17] and others' studies[6,8,9,16-22]. However, available models, including new humanized
57 mouse models that contain injected astrocyte[23], or express human IL-34 to support better development

58 of microglia-like cells[23-26], do not include all three types of human CNS glia (microglia, astrocytes, and
59 oligodendroglia) and donor-matched human immune cells.
60
61 Recently, we and others demonstrated that human microglia and astrocytes can engraft in the brains of
62 immunodeficient mice, retain function, and interact with mouse neuronal synapses[27-29]. Here we report
63 that we have successfully constructed glia-immune humanized mice, which achieve robust engraftment
64 of *both* human immune cells in the periphery and donor-matched human microglia-like cells, astrocytes,
65 and oligodendroglia in mouse brains. Our glia-immune humanized mice support robust HIV infection both
66 in the periphery and in the CNS. Chronic immune activation and neuroinflammation are strongly
67 associated with increased rates of HIV-associated neurocognitive disorders[30]. We also observed
68 elevated inflammation and transcriptomic changes in human glia cells within the brains of infected mice,
69 including elevated type I interferon (IFN-I) responses, which mimic human conditions. Our model provides
70 a unique opportunity to investigate the interplay between HIV infection, chronic immune activation, and
71 neuroinflammation within a physiologically relevant CNS environment.
72
73 **Results**
74 **The Glia-immune humanized NSG mouse model supports the development of human immune**
75 **cells**
76 To study HIV CNS infection and the role of human glia in CNS inflammation, we developed a novel glia-
77 immune humanized mouse model. In this model, mice are reconstituted with donor-matched human glial
78 cells in the brain and a human immune system in periphery and lymphoid tissues. As shown in **Fig. 1A**,
79 neonatal immunodeficient NSG mice (NOD.Cg-*Prkdc*^{scid}*Il2rg*^{tm1Wjl}/SzJ) were injected with donor-matched
80 fetal liver-derived CD34+ HSCs (via intrahepatic injection) and fetal brain-derived astrocytes and
81 oligodendroglia (via intracranial injection, as detailed in[27]). For glial transplantation, astrocytes and
82 oligodendroglia were injected into the neonatal mouse brain at 4 injection sites, including the striatum

83 and thalamus bilaterally. Mice were bled and the reconstitution level was assessed 18 weeks after
84 transplant.
85
86 We first determined whether glia-immune humanized mice exhibit similar levels of human immune
87 reconstitution when compared to primary human peripheral blood mononuclear cells (PBMCs) from
88 healthy donors and the Bone marrow- Liver-Thymus (BLT) humanized mouse, a well characterized
89 humanized mouse model that supports robust immune reconstitution and allows for comprehensive
90 studies in HIV immunity. The BLT humanized mouse model is key for seminal studies of cell and gene
91 therapy for HIV cure[7,9,31-43], studies in HIV latency[10,11,44,45] and mechanistic studies of HIV
92 immunopathogenesis [16,40,41,46-50]. We performed a comparative analysis among humanized glia-immune
93 mice, BLT mice, and fresh human PBMCs of the percentage of human CD45+ cells in the PBMCs and
94 the distribution of human immune cell subsets, including T cells (CD3+), B cells (CD19+), monocytes
95 (CD14+) using flow cytometry.
96
97 In the glia-immune mice, we observed similar level of CD45+% cells among the PBMCs as compared to
98 BLT mice **(Fig. 1B).** Within the human CD45+ lymphocytes of the glia-immune mice, we observed
99 successful development of T cells (CD3+), B cells (CD19+) and monocytes (CD14+), at levels similar to
100 primary human PBMCs from healthy donors**(Fig 1C).** Glia-immune humanized mice showed significantly
101 better development of B cells and monocytes compared to BLT mice**(Fig 1C).** Among the T cell subsets,
102 70.3% of T cells in the glia-immune humanized mice were CD4+ and 21.7% were CD8+, similar to primary
103 human PBMCs and to BLT mice **(Fig 1D).** These results suggest that glia-immune humanized mice
104 support robust development of multiple hematopoietic lineages, resembling human PBMCs more closely
105 than the humanized BLT mice.
106
107 **Reconstitution of human microglia-like cells, astrocytes, and oligodendroglia**

108 To examine the reconstitution of human glia in host mouse brain, we performed IHC analyses of
109 xenografted mouse brains at 26 weeks post reconstitution. As shown in **Fig. 2A**, we observed widespread
110 engraftment of human glia in the brains, including astrocytes (hNuclei+Sox9+), microglia-like cells
111 (huNuclei+Iba1+) (**Fig. 2B**), and human oligodendroglia (huNuclei+Olig2+) (**Fig. 2C**). RNAscope
112 confirmed the engraftment of human microglia-like cells (hCsf1r+) in the cerebral cortex, hippocampus,
113 and meninges (**Fig. 2D**), and human astrocytes (hSlc1a3+) in the cerebral cortex (CTX), hippocampus
114 (Hippo) and striatum (STR) (**Fig. 2E**). As shown in the quantification in **Fig. 2F, G, H**, consistently high
115 and widespread engraftment of human glial cells (astrocytes, microglia and OLG) were observed in
116 multiple brain regions, including the CTX, corpus callosum (CC), Hippo and STR. Although we did not
117 directly transplant human microglia, Iba1+Csf1r+ human microglia-like cells were nonetheless detected
118 in the xenografted mouse brains, likely originating from HSCs. The presence of microglia-like cells,
119 coupled with the widespread engraftment of human astrocytes and oligodendroglia, establishes our
120 model as a more comprehensive platform for neuroimmune research than traditional HSC
121 transplantation-based humanized mouse models, which do not contain human astrocytes or
122 oligodendroglia cells.
123
124 **Robust HIV replication in periphery and brains of Glia-immune humanized mice**
125 To examine if glia-immune humanized mice support robust HIV infection, mice were constructed and,
126 following confirmation of successful immune reconstitution 12 weeks after transplantation, were either
127 left uninfected or infected with the R5 tropic HIV-1_{CH040} via intravenous injection[6,7,14,15]. The levels of HIV
128 replication over time were determined on plasma samples collected at multiple time points post-infection
129 (Weeks 2, 4, 6, 8, and 10). The viral load in the plasma showed a progressive increase, with HIV RNA
130 levels ranging from 1.2×10^6 copies/ml at Week 2 to 6×10^6 copies/ml at Week 10, demonstrating
131 sustained viral replication over the 10-week observation period (**Fig. 3A**), similar to what was observed
132 in BLT humanized mice model [51].
133

134 In addition to plasma, the viral replication in lymphoid and central nervous system (CNS) tissues were
135 assessed. 12 weeks after HIV infection, mice were euthanized and perfused with PBS, with the left
136 hemisphere of the brain fixed for IHC and RNAscope, while the right hemisphere was processed for flow
137 cytometry, real time PCR, and RNAseq analysis. HIV RNA was detected in the blood, spleen, and PBS-
138 perfused brain tissues using quantitative real-time PCR. The data revealed substantial HIV RNA
139 expression in all three tissues, with cycle threshold (Cq) values ranging from 26.34 to 42.20 in the blood,
140 20.18 to 30.12 in the spleen, and 26.46 to 33.37 in the brain. As shown in **Fig 3B**, the HIV-RNA analysis
141 was normalized to HPRT1 as the housekeeping gene. These findings confirm robust and widespread
142 HIV replication in both lymphoid tissues and the brain, indicating the model's suitability for studying HIV
143 dynamics in peripheral and CNS compartments.
144
145 **HIV infection induces peripheral immune activation, elevated type I IFN responses, CNS glia**
146 **reactivity and interferon response gene activation**
147 HIV infection-mediated chronic inflammation is well documented in PLWH and in infected humanized
148 mice [13,16,52]. Using flow cytometry, we analyzed the expression of key activation marker CD38 and
149 exhaustion marker PD-1 on T cells from uninfected and infected glia-immune humanized mice. As shown
150 **in Fig 4**, activation marker CD38 and exhaustion marker PD-1, were both markedly increased on CD4+
151 and CD8+ T cells in blood (**Fig 4A-D**) and spleen (**Fig 4 E-H**) of HIV infected mice as compared to
152 uninfected mice.
153
154 In addition, we observed that infected mice showed significantly elevated levels of the Type I IFN
155 response gene (ISG) MX1 in blood, spleen and brain tissues compared to uninfected controls (**Fig. 5A**),
156 mirroring observations in PLWH[53-55] and reflecting the ongoing immune activation in response to
157 persistent HIV replication. Immunohistochemistry (IHC) further confirmed increased human MX1
158 expression in the brains of infected mice (**Fig. 5B**). We observed increased density of hMX1+ glial cells
159 in corpus collosum, cortex, hippocampus and thalamus of the glia immune humanized mice (**Fig.5C-F**).

160

161 To identify which CNS cell type(s) upregulate MX1 expression during HIV infection, we co-stained MX1
162 with Iba1 (microglia), GFAP (astrocytes), and Olig2 (oligodendroglia) (**Fig. 5G, 5H**). Surprisingly, we
163 observed extensive colocalization of MX1 with Olig2 (**Fig 5H**), whereas colocalization with Iba1 or
164 GFAP was minimal (**Fig 5G**). These findings suggest that oligodendroglia is the predominant cell type
165 increasing MX1 expression in HIV-infected brains. Although oligodendroglia are not known to be
166 directly infected, secreted signals from infected cells may indirectly induce oligodendroglial MX1
167 upregulation. This oligodendroglial interferon response may contribute to neural circuit dysfunction and
168 cognitive impairment[3], representing an understudied area that can be further investigated using our
169 model.

170

171 **HIV infection leads to microgliosis and astrogliosis in the glia-immune mouse brain.**

172 To determine if HIV infection disturbs brain homeostasis, we examined the status of microglia and
173 astrocytes in these mice. As key regulators of central nervous system homeostasis, microglia and
174 astrocytes function as the brain's primary immune responders and increase in their cell density is
175 indicative of a reactive state, often associated with neuroinflammation and neuropathology [56 57]. We
176 quantified microglia density (Iba1+ cells) (**Fig. 6A**) and reactive astrocyte density (GFAP+ cells) (**Fig. 6B**)
177 in four brain regions: the cortex, corpus callosum, hippocampus, and thalamus. Microglia density
178 increased across various brain regions, with a significant elevation in the hippocampus and thalamus
179 compared to control (**Fig. 6C-F**). Similarly, the density of reactive astrocytes also increased in the
180 examined brain regions, with a significant elevation in the corpus callosum and hippocampus compared
181 to control (**Fig. 6G-J**). These findings suggest that HIV infection induces microgliosis and astrogliosis,
182 which may contribute to disruptions in brain homeostasis.

183

184 **Bulk RNA seq reveals elevation in the expression of Interferon Stimulated genes in HIV infected**
185 **brain samples**

186 Bulk RNA-seq and analysis using the *human* reference genomes using brain samples from HIV-infected
187 versus uninfected subjects revealed a striking induction of type I ISGs and associated antiviral pathways
188 in human glial cells from infected mice(**Fig. 7**). Volcano plot analysis (**Fig. 7A**) identified multiple
189 significantly upregulated ISGs (e.g., OAS3, ISG15, IFI44, IFI44L, IFIT3) alongside classical interferon-
190 regulatory factors (IKZF2, IFNGR1), suggesting a heightened antiviral state in the HIV-infected brain.
191 Network analysis of differentially expressed genes (**Fig. 7B**) highlighted a large, interconnected module
192 of upregulated nodes (red) enriched for interferon-associated factors, whereas a cluster of downregulated
193 genes (blue) encompassed components implicated in transcriptional regulation (ZNF652, IKZF2),
194 metabolic genes (ACSS2, DUT, STIM1) and epigenetic control (EP300). Consistent with these
195 observations, gene set enrichment analysis (**Fig. 7C**) demonstrated that upregulated genes were
196 significantly overrepresented in pathways related to "Interferon alpha/beta signaling," "PKR-mediated
197 signaling," and "ISG15 antiviral mechanisms."

198 **Discussion**

199 Current humanized mouse models, while invaluable for studying peripheral HIV infection, have been
200 limited in their utility to understand CNS infection due to the lack of matched human glia in the brain.
201 Glia, including microglia, astrocytes and oligodendroglia, are essential mediators of CNS homeostasis
202 and immune responses, and their dysfunction in the setting of HIV infection is implicated in neurological
203 complications [3,58,59]. By incorporating donor-matched glial cells, our model supports robust engraftment
204 of astrocytes, oligodendroglia, and microglia-like cells, and simultaneous robust peripheral immune
205 reconstitution of donor matched HSCs. Our model provides a unique platform to investigate HIV
206 infection that spans peripheral organs and the CNS.

207 Our data demonstrated that our model support robust and persistent HIV replication in the peripheral
208 blood, lymphoid tissues and in the brain. The elevated proinflammatory gene expression in both the
209 periphery and brain underscores the potent immunopathological effects of HIV infection. Specifically,

210 bulk RNA sequencing of brain tissues demonstrated upregulation of type I ISGs and inflammasome-
211 associated genes in human glial cells. Importantly, we observed activation of glia in HIV infected
212 animals, including in oligodendroglial cells and astrocytes that are not key reservoirs of HIV, suggesting
213 that bystander activation of glial cells may play key role in CNS inflammation and HIV-associated
214 neurocognitive disorders (HAND)[60]. Interestingly, in brains of infected glia-immune humanized mice, we
215 also observed several down regulated genes that are related to astrocytes and glia metabolism. For
216 example, STIM1 is involved in calcium signaling, which is essential for astrocyte and microglial
217 responses to inflammatory stimuli[61,62]. Downregulation of STIM1 suggests an impairment in calcium
218 signaling pathways, potentially leading to glial dysfunction and contributing to neuroinflammation[63].
219 Similarly, decreased ACSS2 levels could affect neuronal energy metabolism and histone acetylation,
220 impacting neuronal function and memory formation[64-66]. Therefore, our model offers a powerful platform
221 to investigate the molecular mechanisms of HIV-driven neuroinflammation and glial dysfunction in the
222 brain.

223 The ability of this glia-immune humanized mouse model to recapitulate HIV infection and inflammation in
224 the CNS offers a valuable tool for testing curative and neuroprotective interventions. Our model supports
225 a full range of biochemical, imaging, and physiological techniques, creating a robust platform for
226 translational research on neuro-immune interactions in HIV CNS comorbidities and other CNS diseases.
227 In addition, throughout the seven-month study period, we did not observe graft-versus-host disease
228 (GVHD) in our glia-immune humanized mice, highlighting the stability and tolerability of the dual
229 transplant methods.
230

231 In summary, our glia-immune humanized mouse model fills a critical gap in HIV research by integrating
232 donor-matched human glia and a functional human immune system. Our findings highlight the capacity
233 of these mice to support HIV replication within both peripheral and CNS tissues, mirroring key features
234 of human HIV neuropathogenesis. In future work, deeper single-cell analyses and spatial transcriptomic

235 approaches can further delineate the molecular interaction among astrocytes, oligodendrocytes,
236 microglia, neurons, and peripheral immune cells during HIV infection.
237

238 **Materials and Methods**

239 **Isolation of human astrocyte and oligodendroglial cells**

240 Fetal human brain cells were isolated from ~18 weeks old human fetal brains obtained at abortion
241 following a previous protocol[67]. Briefly, human fetal brains were chopped into small pieces using a razor
242 blade and enzymatically dissociated with papain. Dissociated cells were plated in a T75 flask and
243 maintained in a serum-containing culture medium. Three days later, unwanted cells such as neurons
244 were depleted by mechanical shaking. Remaining cells were maintained in culture until transplantation.
245 This method will enrich both human astrocytes and oligodendroglial cells.
246

247 **Generation of novel glia-immune humanized mouse**

248 We developed a novel glia-immune humanized mouse model, where the mice were reconstituted with
249 donor-matched human glial cells in the brain and a human immune system in the peripheral and lymphoid
250 tissues. In brief, immunodeficient NSG mice (NOD.Cg-Prkdc^scid Il2rg^tm1Wjl/SzJ) were injected with
251 0.5 million donor-matched, fetal liver-derived CD34+ HPSCs via intrahepatic injection and 400,000 fetal
252 brain-derived astrocytes and oligodendroglial cells via intracranial injection at four sites in the subcortical
253 regions of the brain, including the striatum and thalamus bilaterally[27]. Fourteen weeks post-reconstitution,
254 successful immune reconstitution was confirmed in the peripheral blood of the humanized mice, with
255 detectable levels of human T cells, B cells, and monocytes. Once reconstitution was verified, the mice
256 were infected with 500 ng of HIV-1_{CH040}.
257

258 **Infection of mice and quantification of viral loads**

259 Glia-immune humanized mice were inoculated with HIV-1 CH040 [68] (500 ng of p24 per mouse) via retro-
260 orbital injection under general anesthesia. The mice were monitored for a period of 10 weeks following

261 infection. To assess HIV plasma viremia every two weeks, viral RNA was extracted from plasma samples,
262 and a one-step real-time PCR was conducted using the TaqMan RNA-to-Ct 1-Step kit (Thermo Fisher
263 Scientific, USA). PCR amplification was performed with the following primers and probe:
264 CH040 forward primer: CAATGGCAGCAATTTTACCA
265 CH040 reverse primer: GAATGCCGAATTCCTGCTTGA
266 CH040 dye-labeled probe: 5' [FAM]- CCCACCAACAGGCGGCCTTCACTG-[NFQ]- 3'
267
268 **Nucleic acid isolation and real time PCR**
269 To assess the expression levels of the Type 1 interferon (IFN) response gene, MX1, and cell-associated
270 HIV RNA, RNA was extracted from harvested cells following the manufacturer's protocol (Qiagen). cDNA
271 was synthesized using the High-Capacity cDNA Reverse Transcription Kit (Thermo Fisher Scientific,
272 USA). For the quantification of MX1 and HPRT1, TaqMan Gene Expression Assays (Thermo Fisher
273 Scientific, USA) were used with the following probes: Human MX1 (Hs00895608_m1) and Human
274 HPRT1 (Hs01003267_m1). For HIV RNA quantification, the primers and probes specific to the CH040
275 strain, as described above, were utilized.
276
277 **Flow cytometry**
278 Single-cell suspensions prepared from the peripheral blood and spleen of glia-immune humanized mice
279 were stained with the following antibodies: CD45 (clone HI30), CD3 (clone OKT3), CD4 (RPA-T4), CD8
280 (RPA-T8), CD14 (clone 61D3), CD11c (clone 3.9), CD11b (clone ICRF44), CD19 (HIB19), PD-1 (clone
281 EH12.2H7), and CD38 (clone HIT2). To facilitate live cell gating, the LIVE/DEAD Fixable Yellow Dead
282 Cell Stain Kit (Invitrogen, USA) was used. Antibodies for cell surface markers were conjugated to a range
283 of fluorophores, including BV785, BV605, Pacific Blue, Alexa Fluor 700 (AF700), Phycoerythrin (PE),
284 ECD, PE-Cy7, Allophycocyanin (APC), PerCP-Cy5.5, and PE-Cy5 in appropriate combinations. Data
285 acquisition was performed using the LSR Fortessa flow cytometer and FACS Diva software (BD
286 Biosciences), while FlowJo software (version 10.7.2) was used for data analysis.

287

288 **IHC**

289 Glia-immune humanized mice were anesthetized using isoflurane and transcardially perfused with 1×
290 PBS (pH 7.4), followed by fixation with 4% paraformaldehyde (PFA). Brains were removed and post-fixed
291 in 4% PFA at 4 °C overnight. The brains were then transferred into a 30% sucrose solution at 4 °C for
292 two days or until they sank to the bottom of the tube. These brain samples were then embedded in an
293 optimal cutting temperature (OCT) compound (Fisher, cat#23-730-571) and stored at −80 °C until
294 sectioning. Brain tissue was sectioned into 30 μm slices using a Leica cryostat and stored in a
295 cryoprotectant solution (30% sucrose, 1% polyvinylpyrrolidone, and 30% ethylene glycol in 0.1 M
296 phosphate buffer) at −20 °C until further use. For immunostaining, sections were first blocked and
297 permeabilized using a solution of 10% donkey serum and 0.3% Triton X-100 in PBS. Sections were then
298 incubated with primary antibody solutions overnight at 4 °C. The following primary antibodies were used:
299 anti-human nucleus protein (Chemicon, cat#MAB1281, 1:500 dilution), anti-Iba1 (Wako, cat#019-19741,
300 1:500 dilution), anti-Olig2 (Millipore, cat#211F1.1, 1:1000 dilution), anti-Sox9 (R&D, cat#AF3075, 1:1000
301 dilution), anti-GFAP (Dako, cat# Z0334, 1:1000 dilution), and anti-human MX1 (Abcam, cat#ab284603,
302 1:500 dilution).After primary antibody incubation, the sections were washed three times in PBS and
303 incubated at room temperature for 2 hours with secondary antibodies. After three additional washes in
304 PBS, the stained sections were mounted onto Superfrost Plus slides (Fisher, cat#12-550-15), covered
305 with mounting medium (Fisher, cat#H1400NB), and sealed with glass coverslips. Fluorescent imaging
306 was carried out on a Zeiss Apotome epifluorescence microscope with consistent power and exposure
307 settings for all samples processed with the same probe set.

308

309 **RNAscope**

310 Glia-immune humanized mice were transcardially perfused with RNase-free PBS followed by fixation with
311 RNase-free 4% PFA. Brains were removed and post-fixed in 4% PFA for an additional 2 hr at room
312 temperature and then overnight at 4 °C. Brains were dehydrated in RNase-free 30% sucrose, embedded

313 in OCT compound, and cut into 20 μm-thick sections using a Leica cryostat. RNAscope experiments
314 were performed using the RNAscope Multiplex Fluorescent Reagent Kit v2 (ACDBio, cat#323100)
315 according to the manufacturer's protocol. Probes specific to human HIV (cat#1574121-C3), human
316 SLC1A3 (cat#461081-C1), and human CSF1R (cat#310811-C2) were obtained from ACDBio and used
317 for this study. Fluorescent imaging was carried out on a Zeiss Apotome epifluorescence microscope with
318

319 **RNAseq**

320 Total RNA was extracted from humanized mouse brain tissues and prepared for Illumina sequencing
321 following standard protocols. Technical replicate FASTQ files were concatenated, and initial quality
322 assessments were performed using FastQC. Unique molecular identifiers (UMIs) were extracted with
323 UMI-tools, while adapter and low-quality bases were trimmed with Trim Galore!. We then removed
324 genomic contaminants using BBSplit and filtered out rRNA sequences with SortMeRNA. To
325 accommodate reads derived from both mouse and human cells, we constructed a mixed reference by
326 combining Gencode GRCm39 (mouse) and GRCh38 (human) assemblies and annotations, creating a
327 single index for genome alignment. Reads were aligned to this hybrid reference using STAR, followed by
328 transcript quantification in alignment-based mode with Salmon. Aligned reads were sorted and indexed
329 (SAMtools), and UMIs were used for deduplication with UMI-tools, complemented by duplicate marking
330 (picard MarkDuplicates). We then assembled transcripts using StringTie, and coverage tracks (bigWig
331 format) were generated via BEDTools and bedGraphToBigWig. Multiple quality-control checks were
332 performed (RSeQC, Qualimap, dupRadar, and Preseq) to evaluate alignment, duplication rates, and
333 library complexity. Finally, differential expression was assessed using DESeq2, and downstream
334 functional analyses—including Gene Ontology, Reactome pathway enrichment, and additional
335 annotation through clusterProfiler—were conducted in R.
336

337 **Study approval**

338 Peripheral blood mononuclear cells were obtained at UCLA in accordance with UCLA IRB–approved
339 protocols under written informed consent using an IRB-approved written consent form by the UCLA
340 Center for AIDS Research Virology Laboratory and distributed for this study without personal identifying
341 information. Human tissue was obtained from UCLA Pathology Core Laboratory without identifying
342 information and did not require IRB approval for its use. Animal research described in this article was
343 performed under the written approval of the UCLA Animal Research Committee in accordance with all
344 federal, state, and local guidelines. All surgeries were performed under ketamine/xylazine and isoflurane
345 anesthesia, and all efforts were made to minimize animal pain and discomfort.
346

347 **Acknowledgement**

348 We thank UCLA Center for AIDS Research (CFAR) Humanized Mouse Core staff research associate
349 Nianxin Zhong for his assistance in the humanized mice work. This work was funded by the National
350 Institute of Allergy and Infectious Diseases (R01AI172727 to AZ and MDM), the National Institute on
351 Drug Abuse (grant R01DA-52841, R01DA059873 to AZ), National Institute of Health grants P30AI28697
352 (to the UCLA CFAR Virology Core, Gene and Cell Therapy Core, and Humanized Mouse Core) and
353 U19AI149504 (to SGK and Dr. Irvin Chen [UCLA]); the California Institute for Regenerative Medicine
354 (grant TRAN1-14625 to SGK.); California HIV/AIDS Research Program (grant H24BD7817 to WM);
355 UCLA-Charles Drew University (CDU) CFAR (grant AI152501 to WM). This work was also supported by
356 the UCLA AIDS Institute, the James B. Pendleton Charitable Trust, and the McCarthy Family Foundation.
357 The graphic figure was created with BioRender.com.

358 **Figures and Figure legends**

359

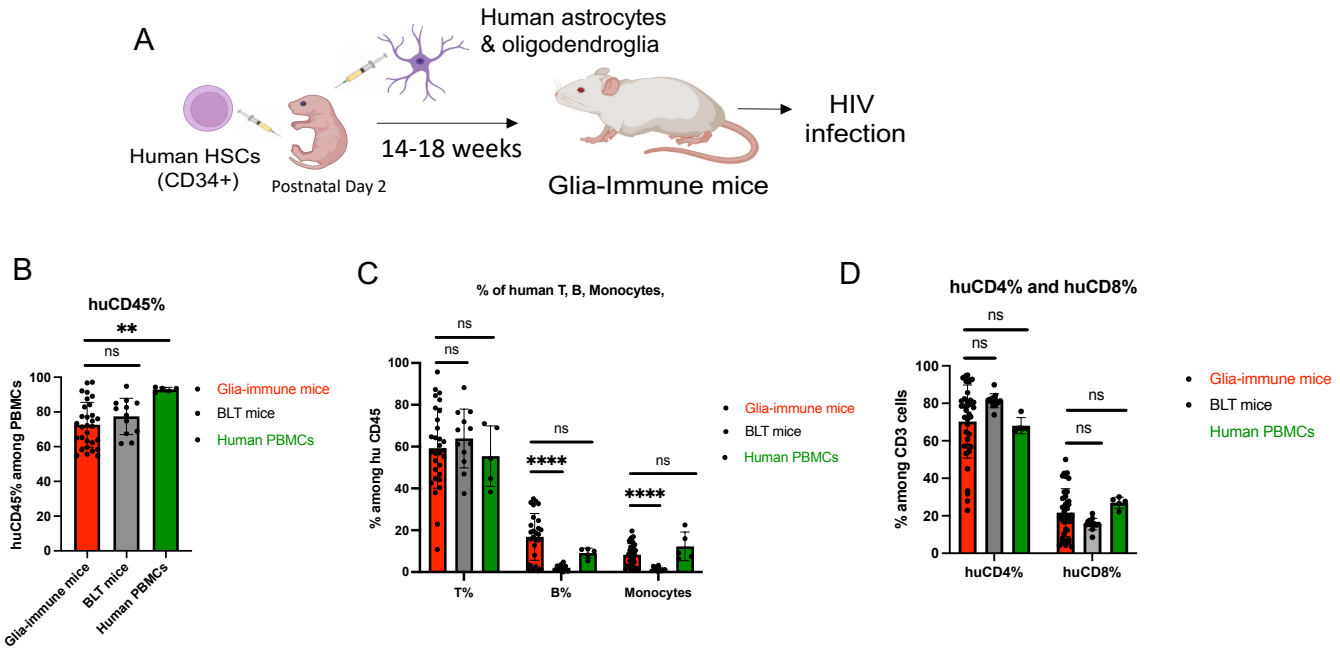

360

361 **Figure 1. Successful engraftment and differentiation of human immune and glia cells in glia-**
362 **immune humanized mice.** A) Human astrocytes and oligodendroglia were transplanted into the
363 subcortical areas of the brains at 1-2mm depth and donor matched human CD34+ HSCs were co-
364 transplanted into the livers of immunodeficient mice at postnatal Day 2. 18 weeks after reconstitution,
365 mice were bled and human immune reconstitution was assessed by flow-cytometry by staining with
366 human antibodies. B) Percentage of huCD45+ cells in PBMCs from the glia-immune humanized mice,
367 humanized BLT mice or primary human PBMCs from healthy donors. C) Percentage of human T cells
368 (huCD3), B cells (huCD19), Monocytes (huCD14) among huCD45 positive cells. D) Percentage of human
369 T-Helper cells (huCD4) and T-cytotoxic cells (huCD8) among T cells. * $p<0.05$, ** $p<0.005$, *** $p<0.0005$,
370 **** $p<0.00005$ by Mann-Whitney test.

371

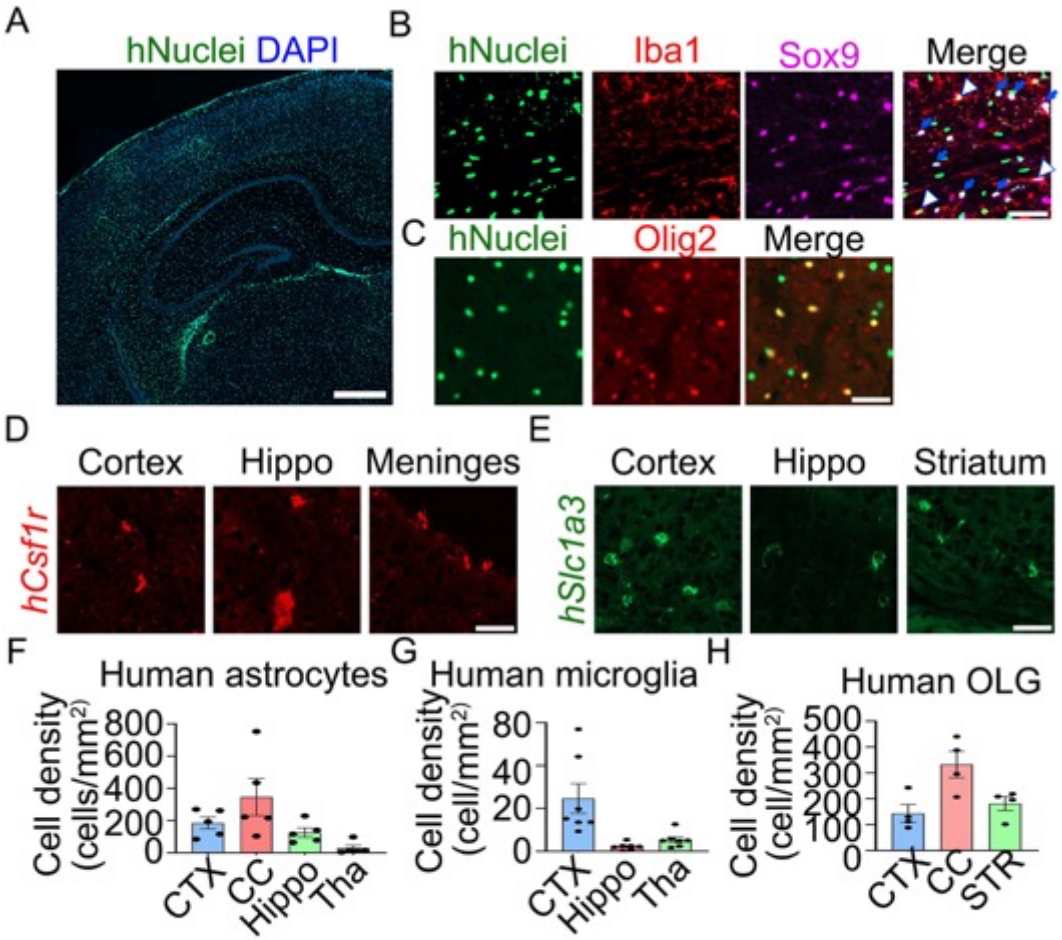

Figure 2. Detection of widespread human glia (astrocytes, oligodendrocyte precursor cells, and microglia-like cells) in the brains of glia-immune humanized mice. A) Human nuclei staining reveals widespread distribution of human cells in the chimeric mouse brain. Scale bar: 500 μm. Green: human nuclei. Blue: DAPI. B) Colocalization of human nuclei with microglia-like cell marker Iba1 and astrocyte marker Sox9 indicates the presence of human microglia-like cells (white arrowhead) and human astrocytes (blue arrow) in the chimeric mouse brain. Scale bar: 50 μm. C) Colocalization of human nuclei with oligodendroglial Olig2 indicates the presence of Oligodendroglia-like cells in the chimeric mouse brain. Scale bar: 50 μm. D) *hCsf1r* RNAscope assay shows human microglia-like cells in the cortex, hippocampus (hippo), and meninges of the chimeric mouse brain. Scale bar: 50 μm. E) *hSlc1a3* RNAscope assay demonstrates the presence of human astrocytes in the cortex, hippocampus, and striatum of the chimeric mouse brain. Scale bar: 50 μm. F) Quantification of the densities of human

384 astrocytes (human nuclei+, Sox9+ double-positive cells) in the cortex (CTX), corpus callosum (CC),
385 hippocampus, and thalamus (Tha) of the chimeric mouse brain. G) Quantification of the densities of
386 human microglia-like cells (human *Csf1r*+ cells) in the cortex, hippocampus, and thalamus of the
387 chimeric mouse brain. H) Quantification of the densities of oligodendroglia cells in the CTX, CC and
388 Stratum (STR).
389

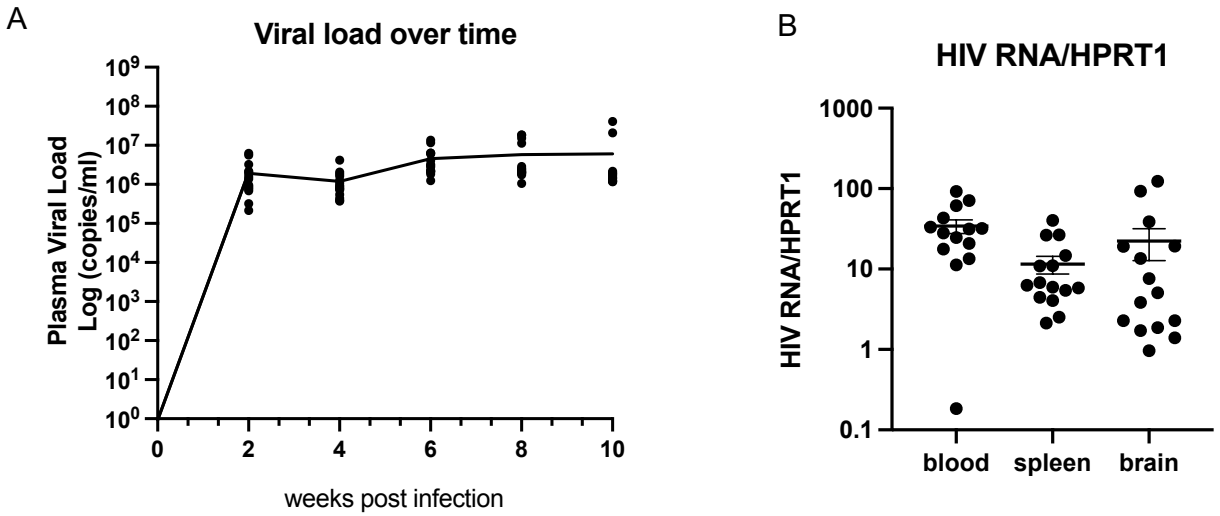

Figure 3. HIV infection in novel glia-immune humanized mice. Glia-immune humanized mice were infected with HIV-1 CH040 (n=16) or mock infected (n=5). (A) Plasma viral load over time in HIV infected glia mice. The X-axis represents time (in weeks) and the y-axis shows the plasma viral load in copies/ml(log scale). (B) 10 weeks after HIV infection, mice were sacrificed, perfused with PBS and tissues were harvested. Viral RNA in blood, spleen and brain was quantified by real-time PCR. HPRT1 is internal control for normalization of gene expression. Data are presented as Mean± SEM.

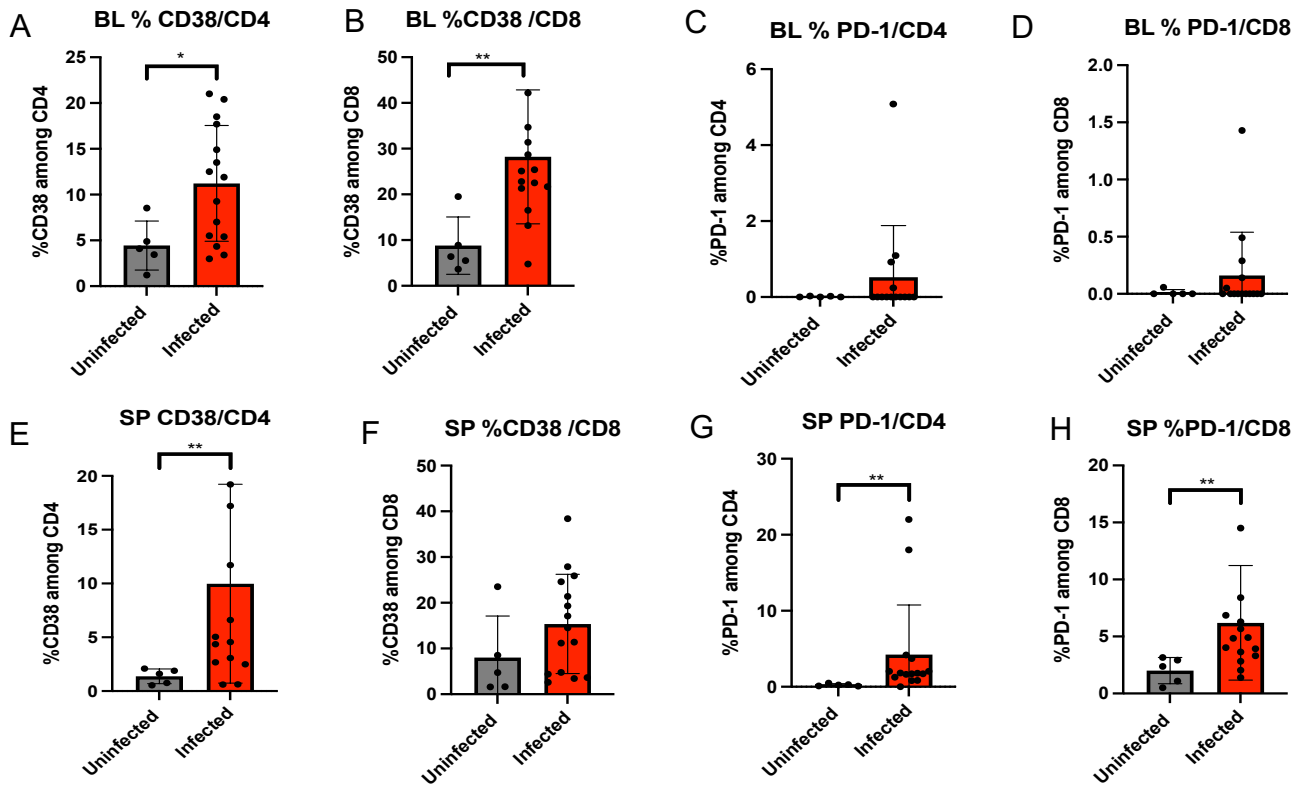

Figure 4. Increased expression of activation and exhaustion markers on T cells in HIV infected glia-immune humanized mice. Mice were infected with HIV-1 CH040, blood (BL) and Spleen (SP) was harvested at the end of 10 week infection. PBMCs and Splenocytes were processed and stained for activation (CD38) (A, B, E, F) and exhaustion markers (PD-1) (C,D,G,J) using Flow-cytometry. Percentage of cells positive for each marker is represented as Mean±S.D. * $p<0.05$, ** $p<0.005$, *** $p<0.0005$, **** $p<0.00005$ by Mann-Whitney test.

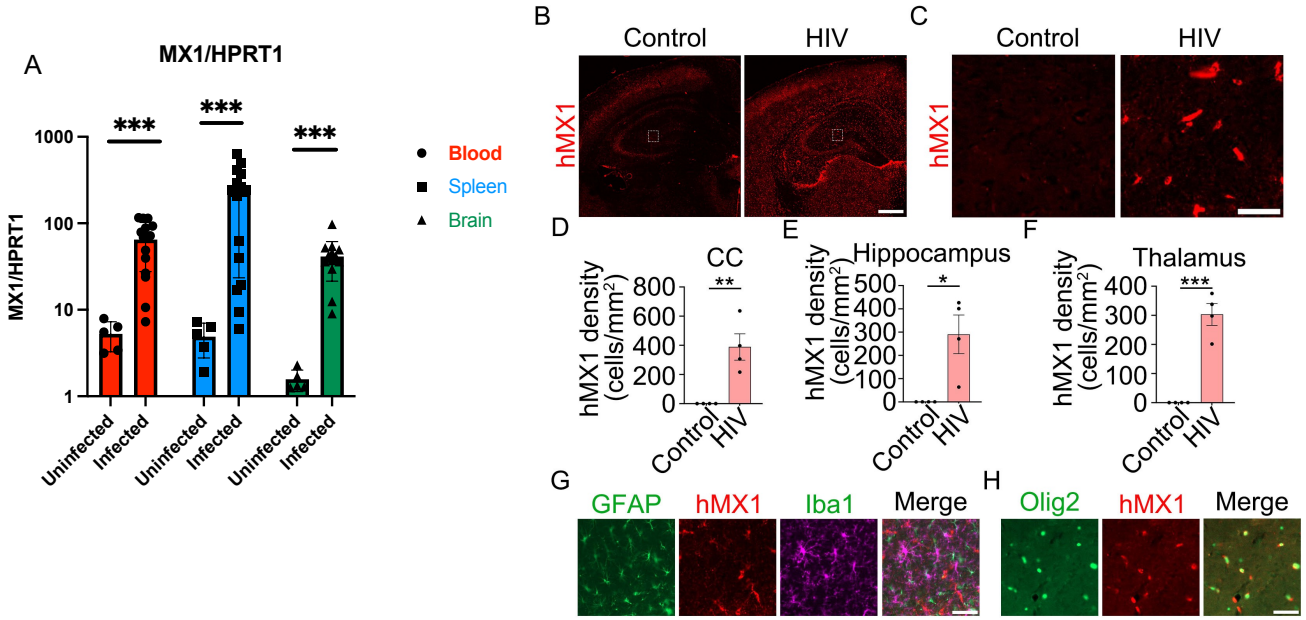

Figure 5: HIV infection induces upregulation of human-specific interferon response gene MX1 in glia-immune humanized mice. A) Interferon stimulated gene -MX1 expression level in blood, spleen and brain as measured by real-time PCR. HPRT1 is internal control for normalization of gene expression. B) Human MX1 (hMX1) staining shows a widespread upregulation of the interferon response in the brains of glia-immune humanized mice following HIV infection. Scale bar: 500 μm. Zoomed in images (dashed rectangular area in B) shows increased human MX1+ cells in the hippocampus of the glia-immune humanized mouse. (C-F). Quantification of the densities of human MX1+ cells in the corpus callosum (CC), cortex, hippocampus, and thalamus of the chimeric mouse brain. G) Limited colocalization of hMX1 (red) with astrocyte (GFAP+ green) or microglia (Iba1+ purple). H) Colocalization (yellow) of hMX1 (red) with Oligodendroglia (Olig2+ in green). (*$p<0.05$, **$p<0.005$, ***$p<0.0005$ by unpaired t-test.)

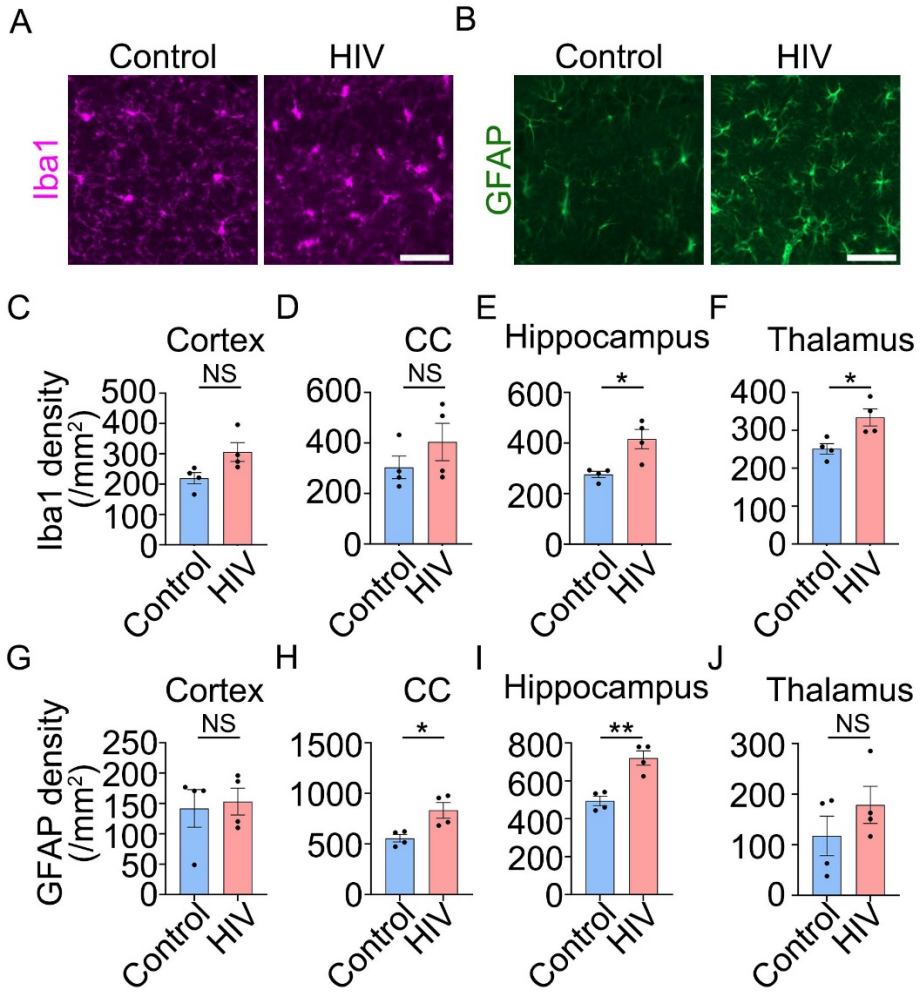

Figure 6. HIV infection leads to microgliosis and astrogliosis in the chimeric mouse brain. A) Iba1 staining in the hippocampus shows that microglia density is increased after HIV infection. Scale bar: 50 μm. B) GFAP staining in the hippocampus shows that reactive astrocytes density is increased after HIV infection. Scale bar: 50 μm.(C - F) Quantification of the density of Iba1+ cells in the cortex, corpus callosum, hippocampus, and thalamus of the chimeric mouse brain. (G - J) Quantification of the density of GFAP+ cells in the cortex, corpus callosum, hippocampus, and thalamus of the chimeric mouse brain. (*$p<0.05$, **$p<0.005$, by unpaired t-test).

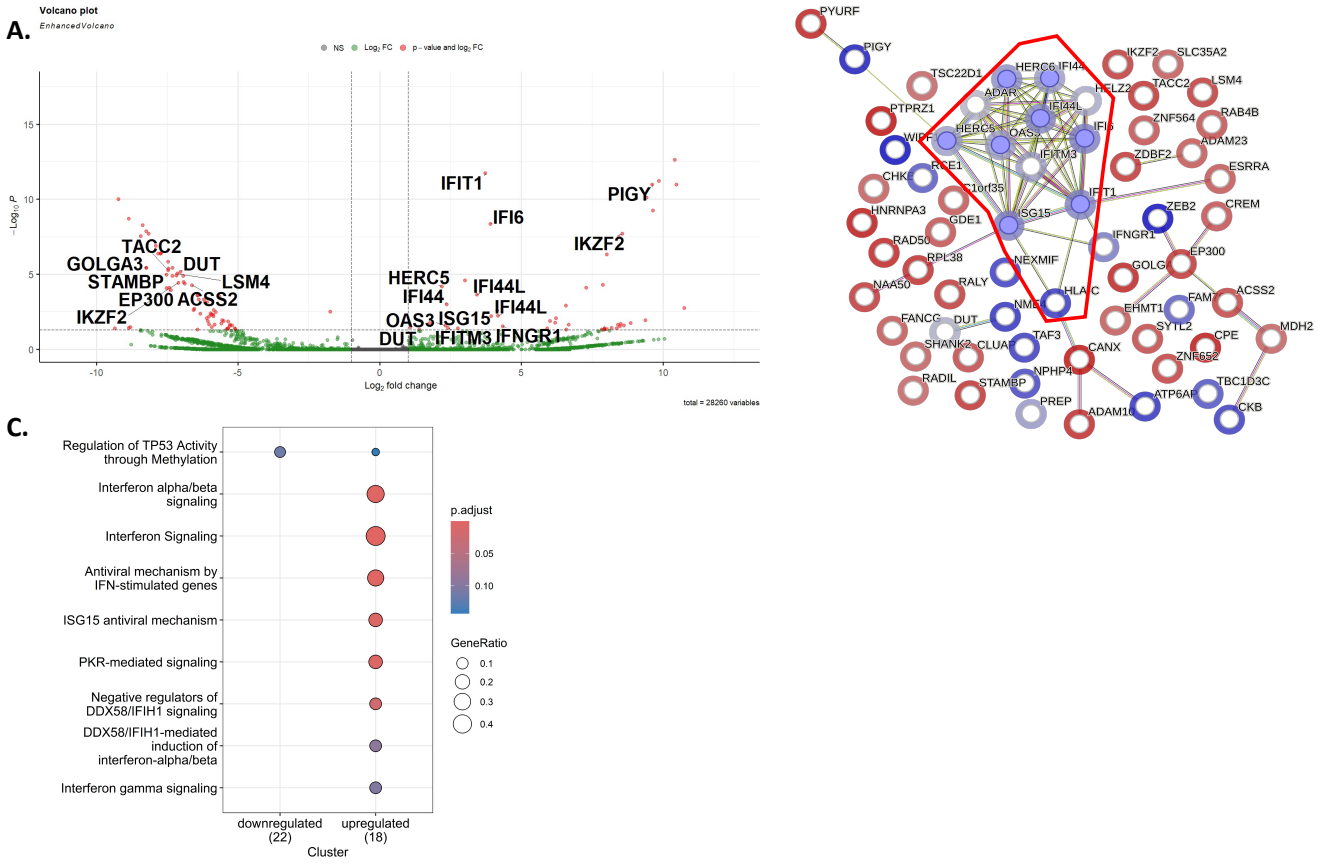

Fig 7. Bulk RNAseq analysis of brains from infected and uninfected glia immune mice. A) Volcano plot showing differential gene expression of infected versus uninfected brains. The x-axis represents the $\log_2$ fold change ($\log_2$FC) in gene expression while the y-axis shows the $-\log_{10}$ p-value. Genes with significant differential expression are highlighted in red. B) Reactome pathway analysis of significantly differentially expressed genes in the brains of infected versus uninfected mice**.** This network visualization displays the interactions between genes with significant changes in expression. Nodes represent individual genes, and edges indicate known or predicted interactions based on pathway data. The network shows a highly interconnected cluster of genes, including ISG15 and OAS1 involved in interferon signaling pathways and the antiviral response. C) Gene enrichment analysis. Red circle highlighting genes involved in interferon signaling.

440 **References**

441

442 1 Borrajo, A., Spuch, C., Penedo, M. A., Olivares, J. M. & Agis-Balboa, R. C. Important role of
443 microglia in HIV-1 associated neurocognitive disorders and the molecular pathways implicated in
444 its pathogenesis. *Ann Med* **53**, 43-69, doi:10.1080/07853890.2020.1814962 (2021).

445 2 Valdebenito, S., Castellano, P., Ajasin, D. & Eugenin, E. A. Astrocytes are HIV reservoirs in the
446 brain: A cell type with poor HIV infectivity and replication but efficient cell-to-cell viral transfer.
447 *J Neurochem* **158**, 429-443, doi:10.1111/jnc.15336 (2021).

448 3 Jensen, B. K., Roth, L. M., Grinspan, J. B. & Jordan-Sciutto, K. L. White matter loss and
449 oligodendrocyte dysfunction in HIV: A consequence of the infection, the antiretroviral therapy or
450 both? *Brain Res* **1724**, 146397, doi:10.1016/j.brainres.2019.146397 (2019).

451 4 Roth, L. M., Akay-Espinoza, C., Grinspan, J. B. & Jordan-Sciutto, K. L. HIV-induced
452 neuroinflammation inhibits oligodendrocyte maturation via glutamate-dependent activation of the
453 PERK arm of the integrated stress response. *Glia* **69**, 2252-2271, doi:10.1002/glia.24033 (2021).

454 5 Veazey, R. S. & Lackner, A. A. Nonhuman Primate Models and Understanding the Pathogenesis
455 of HIV Infection and AIDS. *ILAR J* **58**, 160-171, doi:10.1093/ilar/ilx032 (2017).

456 6 Zhen, A. *et al.* Robust CAR-T memory formation and function via hematopoietic stem cell
457 delivery. *PLoS pathogens* **17**, e1009404, doi:10.1371/journal.ppat.1009404 (2021).

458 7 Zhen, A. *et al.* HIV-specific Immunity Derived From Chimeric Antigen Receptor-engineered Stem
459 Cells. *Molecular therapy : the journal of the American Society of Gene Therapy* **23**, 1358-1367,
460 doi:10.1038/mt.2015.102 (2015).

461 8 Norton, T. D. *et al.* Lentiviral Vector-Based Dendritic Cell Vaccine Suppresses HIV Replication
462 in Humanized Mice. *Molecular therapy : the journal of the American Society of Gene Therapy* **27**,
463 960-973, doi:10.1016/j.ymthe.2019.03.008 (2019).

464 9 Maldini, C. R. *et al.* Dual CD4-based CAR T cells with distinct costimulatory domains mitigate
465 HIV pathogenesis in vivo. *Nature medicine* **26**, 1776-1787, doi:10.1038/s41591-020-1039-5
466 (2020).
467 10 Marsden, M. D. *et al.* Tracking HIV Rebound following Latency Reversal Using Barcoded HIV.
468 *Cell Rep Med* **1**, 100162, doi:10.1016/j.xcrm.2020.100162 (2020).
469 11 Marsden, M. D. *et al.* In vivo activation of latent HIV with a synthetic bryostatin analog effects
470 both latent cell "kick" and "kill" in strategy for virus eradication. *PLoS pathogens* **13**, e1006575,
471 doi:10.1371/journal.ppat.1006575 (2017).
472 12 Carrillo, M. A. *et al.* Stem cell-derived CAR T cells show greater persistence, trafficking, and viral
473 control compared to ex vivo transduced CAR T cells. *Molecular therapy : the journal of the*
474 *American Society of Gene Therapy* **32**, 1000-1015, doi:10.1016/j.ymthe.2024.02.026 (2024).
475 13 Mu, W., Patankar, V., Kitchen, S. & Zhen, A. Examining Chronic Inflammation, Immune
476 Metabolism, and T Cell Dysfunction in HIV Infection. *Viruses* **16**, doi:10.3390/v16020219 (2024).
477 14 Mu, W. *et al.* Autophagy inducer rapamycin treatment reduces IFN-I-mediated Inflammation and
478 improves anti-HIV-1 T cell response in vivo. *JCI insight* **7**, doi:10.1172/jci.insight.159136 (2022).
479 15 Mu, W. *et al.* Oral Combinational Antiretroviral Treatment in HIV-1 Infected Humanized Mice. *J*
480 *Vis Exp*, doi:10.3791/63696 (2022).
481 16 Zhen, A. *et al.* Targeting type I interferon-mediated activation restores immune function in chronic
482 HIV infection. *The Journal of clinical investigation* **127**, 260-268, doi:10.1172/JCI89488 (2017).
483 17 Zhen, A. *et al.* Stem-cell Based Engineered Immunity Against HIV Infection in the Humanized
484 Mouse Model. *Journal of visualized experiments : JoVE*, doi:10.3791/54048 (2016).
485 18 Victor Garcia, J. Humanized mice for HIV and AIDS research. *Current opinion in virology* **19**,
486 56-64, doi:10.1016/j.coviro.2016.06.010 (2016).

487 19 Marsden, M. D. Benefits and limitations of humanized mice in HIV persistence studies.
488 *Retrovirology* **17**, 7, doi:10.1186/s12977-020-00516-2 (2020).
489 20 Rogers, G. L. *et al.* Reprogramming human B cells with custom heavy-chain antibodies. *Nat*
490 *Biomed Eng*, doi:10.1038/s41551-024-01240-4 (2024).
491 21 Hofer, U. *et al.* Pre-clinical modeling of CCR5 knockout in human hematopoietic stem cells by
492 zinc finger nucleases using humanized mice. *The Journal of infectious diseases* **208 Suppl 2**,
493 S160-164, doi:10.1093/infdis/jit382 (2013).
494 22 Mu, W. a. R., Valerie and Martin, Heather and Carrillo, Mayra and Hamid, Philip and Lizarraga,
495 Miguel and Yang, Otto O. and Jamieson, Beth and Kitchen, Scott G. and Zhen, Anjie. . Induction
496 of Autophagy Reduces IFN-I Mediated Inflammation and Restores Anti-HIV-1 T Cell Response
497 in vivo. *Cell Reports Sneak Peek*, doi:http://dx.doi.org/10.2139/ssrn.3895931 (2021).
498 23 Lutgen, V. *et al.* HIV infects astrocytes in vivo and egresses from the brain to the periphery. *PLoS*
499 *pathogens* **16**, e1008381, doi:10.1371/journal.ppat.1008381 (2020).
500 24 Zhang, J. *et al.* Human Microglia Extensively Reconstitute in Humanized-BLT Mice With Human
501 Interleukin-34 Transgene and Support HIV-1 Brain Infection. *Frontiers in immunology* **12**, 672415,
502 doi:10.3389/fimmu.2021.672415 (2021).
503 25 Mathews, S. *et al.* Human Interleukin-34 facilitates microglia-like cell differentiation and
504 persistent HIV-1 infection in humanized mice. *Mol Neurodegener* **14**, 12, doi:10.1186/s13024-
505 019-0311-y (2019).
506 26 Waight, E. *et al.* Animal models for studies of HIV-1 brain reservoirs. *Journal of leukocyte biology*
507 **112**, 1285-1295, doi:10.1002/JLB.5VMR0322-161R (2022).
508 27 Li, J. *et al.* Conservation and divergence of vulnerability and responses to stressors between human
509 and mouse astrocytes. *Nature communications* **12**, 3958, doi:10.1038/s41467-021-24232-3 (2021).

510 28 Mancuso, R. *et al.* Stem-cell-derived human microglia transplanted in mouse brain to study human
511 disease. *Nat Neurosci* **22**, 2111-2116, doi:10.1038/s41593-019-0525-x (2019).
512 29 Fattorelli, N. *et al.* Stem-cell-derived human microglia transplanted into mouse brain to study
513 human disease. *Nat Protoc* **16**, 1013-1033, doi:10.1038/s41596-020-00447-4 (2021).
514 30 Hong, S. & Banks, W. A. Role of the immune system in HIV-associated neuroinflammation and
515 neurocognitive implications. *Brain Behav Immun* **45**, 1-12, doi:10.1016/j.bbi.2014.10.008 (2015).
516 31 Shimizu, S. *et al.* RNAi-Mediated CCR5 Knockdown Provides HIV-1 Resistance to Memory T
517 Cells in Humanized BLT Mice. *Molecular therapy. Nucleic acids* **4**, e227,
518 doi:10.1038/mtna.2015.3 (2015).
519 32 Yi, G. *et al.* CCR5 Gene Editing of Resting CD4(+) T Cells by Transient ZFN Expression From
520 HIV Envelope Pseudotyped Nonintegrating Lentivirus Confers HIV-1 Resistance in Humanized
521 Mice. *Molecular therapy. Nucleic acids* **3**, e198, doi:10.1038/mtna.2014.52 (2014).
522 33 Anthony-Gonda, K. *et al.* Multispecific anti-HIV duoCAR-T cells display broad in vitro antiviral
523 activity and potent in vivo elimination of HIV-infected cells in a humanized mouse model. *Science*
524 *translational medicine* **11**, doi:10.1126/scitranslmed.aav5685 (2019).
525 34 Daharsh, L., Zhang, J., Ramer-Tait, A. & Li, Q. A Double Humanized BLT-mice Model Featuring
526 a Stable Human-Like Gut Microbiome and Human Immune System. *Journal of visualized*
527 *experiments : JoVE*, doi:10.3791/59773 (2019).
528 35 Claiborne, D. T. *et al.* Immunization of BLT Humanized Mice Redirects T Cell Responses to Gag
529 and Reduces Acute HIV-1 Viremia. *Journal of virology* **93**, doi:10.1128/JVI.00814-19 (2019).
530 36 Lavender, K. J. *et al.* An advanced BLT-humanized mouse model for extended HIV-1 cure studies.
531 *AIDS (London, England)* **32**, 1-10, doi:10.1097/QAD.0000000000001674 (2018).

532 37 Marsden, M. D. & Zack, J. A. Humanized Mouse Models for Human Immunodeficiency Virus
533 Infection. *Annual review of virology* **4**, 393-412, doi:10.1146/annurev-virology-101416-041703
534 (2017).
535 38 Karpel, M. E., Boutwell, C. L. & Allen, T. M. BLT humanized mice as a small animal model of
536 HIV infection. *Current opinion in virology* **13**, 75-80, doi:10.1016/j.coviro.2015.05.002 (2015).
537 39 Wahl, A. & Victor Garcia, J. The use of BLT humanized mice to investigate the immune
538 reconstitution of the gastrointestinal tract. *J Immunol Methods* **410**, 28-33,
539 doi:10.1016/j.jim.2014.06.009 (2014).
540 40 Seung, E. *et al.* PD-1 blockade in chronically HIV-1-infected humanized mice suppresses viral
541 loads. *PloS one* **8**, e77780, doi:10.1371/journal.pone.0077780 (2013).
542 41 Dudek, T. E. & Allen, T. M. HIV-specific CD8(+) T-cell immunity in humanized bone marrow-
543 liver-thymus mice. *The Journal of infectious diseases* **208 Suppl 2**, S150-154,
544 doi:10.1093/infdis/jit320 (2013).
545 42 Ringpis, G. E. *et al.* Engineering HIV-1-resistant T-cells from short-hairpin RNA-expressing
546 hematopoietic stem/progenitor cells in humanized BLT mice. *PloS one* **7**, e53492,
547 doi:10.1371/journal.pone.0053492 (2012).
548 43 Vatakis, D. N. *et al.* Using the BLT humanized mouse as a stem cell based gene therapy tumor
549 model. *Journal of visualized experiments : JoVE*, e4181, doi:10.3791/4181 (2012).
550 44 Marsden, M. D. *et al.* HIV latency in the humanized BLT mouse. *Journal of virology* **86**, 339-347,
551 doi:10.1128/JVI.06366-11 (2012).
552 45 Denton, P. W. *et al.* Generation of HIV latency in humanized BLT mice. *Journal of virology* **86**,
553 630-634, doi:10.1128/JVI.06120-11 (2012).

554 46 Garcia-Beltran, W. F. *et al.* Innate Immune Reconstitution in Humanized Bone Marrow-Liver-
555 Thymus (HuBLT) Mice Governs Adaptive Cellular Immune Function and Responses to HIV-1
556 Infection. *Frontiers in immunology* **12**, 667393, doi:10.3389/fimmu.2021.667393 (2021).
557 47 Yan, H., Semple, K. M., Gonzalez, C. M. & Howard, K. E. Bone marrow-liver-thymus (BLT)
558 immune humanized mice as a model to predict cytokine release syndrome. *Transl Res* **210**, 43-56,
559 doi:10.1016/j.trsl.2019.04.007 (2019).
560 48 Crawford, L. B. *et al.* Human Cytomegalovirus Induces Cellular and Humoral Virus-specific
561 Immune Responses in Humanized BLT Mice. *Scientific reports* **7**, 937, doi:10.1038/s41598-017-
562 01051-5 (2017).
563 49 Ginwala, R. *et al.* HTLV-1 Infection and Neuropathogenesis in the Context of Rag1(-/-)gammac(-
564 /-) (RAG1-Hu) and BLT Mice. *Journal of neuroimmune pharmacology : the official journal of the*
565 *Society on NeuroImmune Pharmacology* **12**, 504-520, doi:10.1007/s11481-017-9740-y (2017).
566 50 Cheng, L. *et al.* Blocking type I interferon signaling enhances T cell recovery and reduces HIV-1
567 reservoirs. *The Journal of clinical investigation* **127**, 269-279, doi:10.1172/JCI90745 (2017).
568 51 Honeycutt, J. B. *et al.* T cells establish and maintain CNS viral infection in HIV-infected
569 humanized mice. *The Journal of clinical investigation* **128**, 2862-2876, doi:10.1172/JCI98968
570 (2018).
571 52 Deeks, S. G., Tracy, R. & Douek, D. C. Systemic effects of inflammation on health during chronic
572 HIV infection. *Immunity* **39**, 633-645, doi:10.1016/j.immuni.2013.10.001 (2013).
573 53 Wang, B., Kang, W., Zuo, J., Kang, W. & Sun, Y. The Significance of Type-I Interferons in the
574 Pathogenesis and Therapy of Human Immunodeficiency Virus 1 Infection. *Front Immunol* **8**, 1431,
575 doi:10.3389/fimmu.2017.01431 (2017).

576 54 Thaney, V. E. & Kaul, M. Type I Interferons in NeuroHIV. *Viral Immunol* **32**, 7-14,
577 doi:10.1089/vim.2018.0085 (2019).
578 55 Murira, A. & Lamarre, A. Type-I Interferon Responses: From Friend to Foe in the Battle against
579 Chronic Viral Infection. *Frontiers in immunology* **7**, 609, doi:10.3389/fimmu.2016.00609 (2016).
580 56 Colonna, M. & Butovsky, O. Microglia Function in the Central Nervous System During Health
581 and Neurodegeneration. *Annual review of immunology* **35**, 441-468, doi:10.1146/annurev-
582 immunol-051116-052358 (2017).
583 57 Lee, H. G., Lee, J. H., Flausino, L. E. & Quintana, F. J. Neuroinflammation: An astrocyte
584 perspective. *Science translational medicine* **15**, eadi7828, doi:10.1126/scitranslmed.adi7828
585 (2023).
586 58 Wahl, A. & Al-Harthi, L. HIV infection of non-classical cells in the brain. *Retrovirology* **20**, 1,
587 doi:10.1186/s12977-023-00616-9 (2023).
588 59 Tang, Y. *et al.* Brain microglia serve as a persistent HIV reservoir despite durable antiretroviral
589 therapy. *The Journal of clinical investigation* **133**, doi:10.1172/JCI167417 (2023).
590 60 Ash, M. K., Al-Harthi, L. & Schneider, J. R. HIV in the Brain: Identifying Viral Reservoirs and
591 Addressing the Challenges of an HIV Cure. *Vaccines (Basel)* **9**, doi:10.3390/vaccines9080867
592 (2021).
593 61 Lia, A. *et al.* Rescue of astrocyte activity by the calcium sensor STIM1 restores long-term synaptic
594 plasticity in female mice modelling Alzheimer's disease. *Nature communications* **14**, 1590,
595 doi:10.1038/s41467-023-37240-2 (2023).
596 62 Michaelis, M., Nieswandt, B., Stegner, D., Eilers, J. & Kraft, R. STIM1, STIM2, and Orai1
597 regulate store-operated calcium entry and purinergic activation of microglia. *Glia* **63**, 652-663,
598 doi:10.1002/glia.22775 (2015).

63 Serwach, K. & Gruszczynska-Biegala, J. Target Molecules of STIM Proteins in the Central Nervous System. *Front Mol Neurosci* **13**, 617422, doi:10.3389/fnmol.2020.617422 (2020).

64 Alexander, D. C. *et al.* Targeting acetyl-CoA metabolism attenuates the formation of fear memories through reduced activity-dependent histone acetylation. *Proceedings of the National Academy of Sciences of the United States of America* **119**, e2114758119, doi:10.1073/pnas.2114758119 (2022).

65 Mews, P. *et al.* Alcohol metabolism contributes to brain histone acetylation. *Nature* **574**, 717-721, doi:10.1038/s41586-019-1700-7 (2019).

66 Mews, P. *et al.* Acetyl-CoA synthetase regulates histone acetylation and hippocampal memory. *Nature* **546**, 381-386, doi:10.1038/nature22405 (2017).

67 McCarthy, K. D. & de Vellis, J. Preparation of separate astroglial and oligodendroglial cell cultures from rat cerebral tissue. *J Cell Biol* **85**, 890-902, doi:10.1083/jcb.85.3.890 (1980).

68 Keele, B. F. *et al.* Identification and characterization of transmitted and early founder virus envelopes in primary HIV-1 infection. *Proceedings of the National Academy of Sciences of the United States of America* **105**, 7552-7557, doi:10.1073/pnas.0802203105 (2008).